Preliminary results of aperture area comparison for exo-atmospheric solar irradiance

B. Carol Johnson[*a], Maritoni Litorja[a], James J. Butler[b]
[a]National Institute of Standards and Technology, 100 Bureau Drive, Gaithersburg MD, USA, 20899
[b]National Aeronautics and Space Administration's Goddard Space Flight Center, Greenbelt, MD, USA, 20771

ABSTRACT

Exo-atmospheric solar irradiance measurements made by the solar irradiance community over the past 25 years incorporated limiting apertures measured by a number of metrology laboratories using a variety of techniques. Knowledge of the aperture area is a critical component in the conversion of radiant flux measurements to solar irradiance. An Earth Observing System (EOS)-sponsored international comparison of aperture area measurements of limiting apertures provided by solar irradiance researchers is under way, the effort being executed by the National Institute of Standards and Technology (NIST) in coordination with the EOS Project Science Office. Apertures that have institutional heritage with historical solar irradiance measurements are measured using the absolute aperture measurement facility at NIST. The measurement technique employs non-contact video microscopy using a high-precision stage. The aperture area comparison aims to quantify the relative differences between the participating institutions' aperture area measurements. Preliminary results of the comparison will be reported.

Keywords: Absolute radiometry, aperture area, solar irradiance

1. INTRODUCTION

The radiant flux from the sun is the primary source of energy for the Earth. Photosynthesis, temperature, atmospheric and oceanic dynamics, and the extent of the protective stratospheric ozone layer are all a function of the exo-atmospheric solar irradiance. Solar irradiance monitoring is important for studies of global climate change, paleo-climatic studies, solar physics, and space weather. The solar radiant output is variable both spectrally and temporally, on multiple time scales.[1] For global climate change studies, long-term, decadal changes in solar irradiance are of highest interest. In 1994, the National Research Council, in its publication of research priorities for solar influences on global change, emphasized the importance of solar irradiance measurements by recommending that highest priority be given to "monitoring total and spectral solar irradiance from an uninterrupted, overlapping series of spacecraft radiometers employing in-flight sensitivity tracking."[2]

Satellite instruments have typical on-orbit measurement lifetimes of 5 years. Therefore, the decadal measurement of solar irradiance necessary for studies of the repeatability of solar minimum and maximum levels can only be realized using multiple instruments. For the case of total solar irradiance, which is the radiant energy emitted by the Sun over all spectral regions falling each second on one square meter outside the Earth's atmosphere, on-orbit measurements using electrical substitution radiometers have been acquired since the 1978 launch of the Earth Radiation Budget (ERB) experiment on Nimbus 7. Table 1 lists the past, current, and future, long-term, total solar irradiance satellite instruments and their on-orbit measurement intervals. The historical total solar irradiance database produced from these measurements for several of the instruments in Table 1 is shown in Fig. 1. From the data in Fig. 1, the instrument measurements agree in the relative magnitude of the amplitudes of the 11-year solar cycle differences but disagree up to 7.5 W/m^2 in the absolute decadal level of total solar irradiance. This difference in absolute level is several times the relative difference of 1.3 W/m^2, or 0.1 %, between solar maximum and minima.[3] The observed discrepancies introduce ambiguity in the absolute solar irradiance, forcing the choice of a reference value when producing a composite result from the data in Fig. 1. In addition, the data must be corrected for changes in the radiometer sensitivity, orbit orientation, etc. during the mission, in order to accurately assess absolute changes in the total solar irradiance, as

[*] Correspondence: cjohnson@nist.gov

Proceedings of SPIE Vol. 5151 Earth Observing Systems VIII, edited by William L. Barnes (SPIE, Bellingham, WA, 2003) · 0277-786X/2003/$15.00

indicated, for example, by the value during solar minimum. Radiometrically-speaking, these are small effects, but they have important consequences when separating natural from anthropogenic effects on Earth's climate.[1,3] In 1999, Quinn and Frohlich evaluated the existing data and concluded that the total solar irradiance is stable to within 0.02 % +/- 0.3 %, and they recommended stronger cooperation between the scientific and national metrological communities with the goal of reducing on-orbit measurement uncertainties.[4]

Understanding the differences between absolute total solar irradiance measurements depends on comprehensive pre-launch instrument characterization and careful on-orbit assessment of instrument degradation. Key to pre-launch characterization is the assessment of an instrument's measurement uncertainty budget. For total solar irradiance instruments, this budget typically includes uncertainties in the spacecraft/Sun distance and associated relativistic effects, scattered light, thermal equivalence between cavity applied heating and solar heating, on-board electrical standards, shutter waveform, instrument gain, cavity absorption and its predicted on-orbit degradation, and aperture area. For many satellite instruments, the determination of aperture area is one of the dominant uncertainty components.

Table 1. Long-term, total solar irradiance satellite instruments and data records from 1978 to the present.

Instrument or experiment/platform	Total Solar Irradiance Data Record
Earth Radiation Budget (ERB) Experiment (ERBE)/Nimbus 7	November 16, 1978 to December 13, 1993
Active Cavity Radiometer Irradiance Monitor I (ACRIM I)/Solar Maximum Mission (SMM)	February 16, 1980 to June 1, 1989
Earth Radiation Budget Experiment (ERBE)/Earth Radiation Budget Satellite (ERBS)	October 25, 1984 to present
Earth Radiation Budget Experiment (ERBE)/National Oceanic and Atmospheric Administration 9 Satellite (NOAA 9)	January 23, 1985 to December 20, 1989
Earth Radiation Budget Experiment (ERBE)/ National Oceanic and Atmospheric Administration 10 Satellite (NOAA 10)	October 22, 1986 to December 1, 1987
Active Cavity Radiometer Irradiance Monitor II (ACRIM II)/Upper Atmospheric Research Satellite (UARS)	October 5, 1991 to August 2001
SOlar VAriability experiment 2 (SOVA 2)/EUropean REtrievable CArrier (EURECA)	August 7, 1992 to June 1993
SOLar CONstant (SOLCON)/ATLAS and Hitchhiker	March 24, 1992 to present
Variability of solar IRradiance and Gravity Oscillations (VIRGO)/Solar and Heliospheric Observatory (SOHO)	December 2, 1995 to present
Active Cavity Radiometer Irradiance Monitor III (ACRIM III)/Active Cavity Radiometer Irradiance Monitor SATellite (ACRIMSAT)	April 5, 2000 to present
Total Irradiance Monitor (TIM)/Solar Radiation and Climate Experiment (SORCE)	February 25, 2003 to present
Solar Irradiance Gap Filler (SIGF)/Vegetation Canopy Lidar (VCL) bus	Future instrument
Total Solar Irradiance Sensor (TSIS)/National POlar-orbiting Environmental Satellite System (NPOESS)	Future instrument
SOlar Variability and Irradiance Monitor (SOVIM)/International Space Station (ISS)	Future instrument

It must be pointed out that, although the spread in the results in Fig. 1 is large, up to 0.55 %, the results agree within the uncertainty estimates for the different satellite instruments, which are typically between 0.2 % and 0.3% (k = 1).[3] However, the results point to the existence of one or several systematic causes. In terms of aperture area uncertainty, for this component to be small, < 0.01 % for example, the radius of a precise circular aperture that is 2.5 mm in diameter must be uncertain to less than 0.13 μm. In addition, the effective optical aperture size must be independent of the method used to determine the area and the aperture area must remain constant in time (no oxidation, for example). The realistic assignment of the uncertainty in the pre-launch measurement of aperture area is difficult, and best assessed by a measurement comparison program. In a May 2000 calibration workshop for the Total Irradiance Monitor (TIM) Instrument on the Earth Observing System (EOS) Solar Radiation and Climate Experiment (SORCE), workshop

participants endorsed the idea of holding a comparison program on aperture area measurement with NIST serving as the hub institution.[5] The comparison presented in this paper is in response to that endorsement. It is consistent with the goals of the EOS Calibration/Validation Program [6,7] and complements the previous comparison on bi-directional reflectance.[8] The goal of this comparison is to quantify the relative differences in measurements of aperture area made by or for institutions involved in the on-orbit measurement of total solar irradiance and those made by a national standards laboratory, NIST. To date, apertures have been received from two participating institutions, referred to as A and B in the text below. It is anticipated that apertures will be received from a third and possibly a fourth institution. The results presented in this paper, therefore, should be considered preliminary.

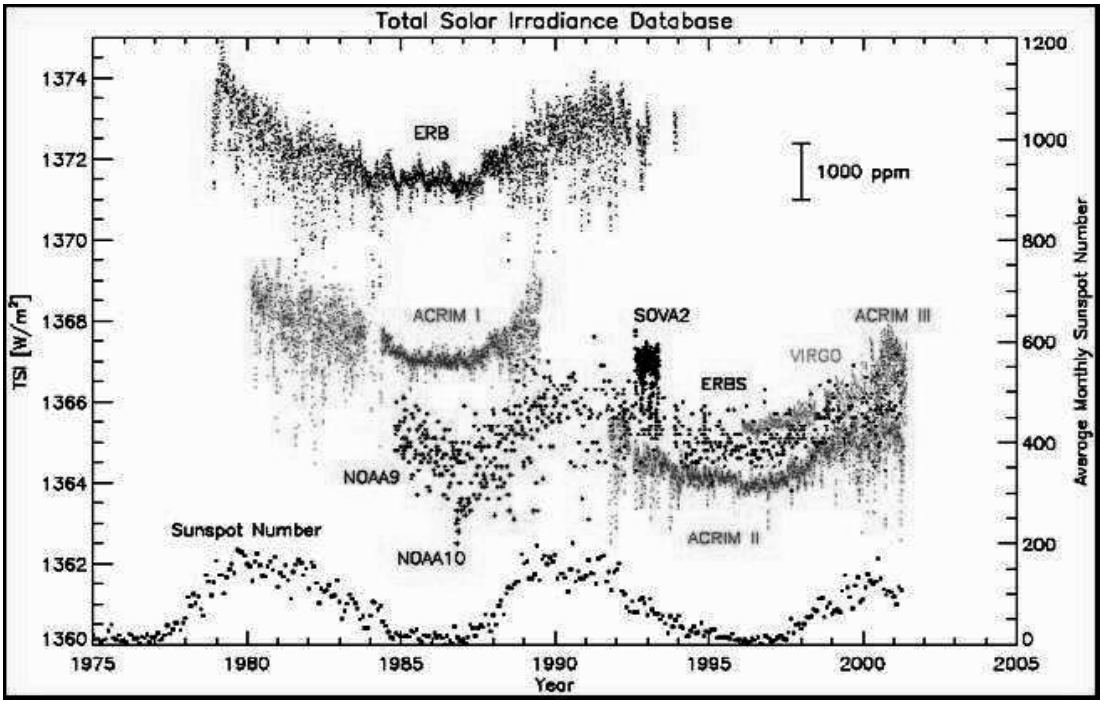

Figure 1. Total solar irradiance measurements made by long-term satellite instruments since 1978. The sunspot number is also shown on this figure to illustrate its correlation with irradiance. [Courtesy of SORCE website: http://lasp.colorado.edu/sorce]

2. METHODOLOGY

2.1 Aperture Measurement Methods

Historically, aperture area has been determined using a variety of contact and non-contact methods. In the contact method, a ball-ended stylus makes mechanical contact with an aperture edge with a force typically 0.06 N, and then travels until the opposing edge is detected.[9,10] Diameter values at several points along the circular aperture are determined. This is commonly used for internal diameter measurement of ring gages or setting rings.[11] Ring gages typically have vertical walls, and this method lends well for those samples. Optical apertures measured with this method require a land, or vertical wall of about 70 μm, to define a point of contact and prevent edge damage from contact with the probe. However, the land reflects light, and results in a focusing effect that makes it difficult to determine the actual optical area. Currently, apertures for radiometry are constructed with knife edges using diamond turning or with very thin edges using electro-deposition. This requires a non-contact method for determining the area.

Several non-contact measurement techniques are currently used to measure knife-edged apertures. One is through the flux ratio method, where the ratio of the radiant flux transmitted through an aperture of known area to that of flux through a test aperture is measured. The ratio of the measured flux is equivalent to the ratio of the areas.[9,12,13] Other

methods are geometric area measurements, such as the optical microtopography sensor described by Stock and Fischer, which utilizes the waist of a laser beam as the probe for the edge.[14] The laser is scanned across the aperture and senses the aperture edge due to the reflected beam. This method requires apertures have a reflectance of greater than 4 %. Lassila *et al*. measure the area of an aperture by determining the ratio of total optical power to irradiance, using a laser beam as the optical source. The aperture is positioned in front of an integrating sphere, where a photodetector is situated, and translated by a stage. The photodetector signal is noted at each incremental position.[15]

For both contact and non-contact methods, accurate measurement of the travel distance of the probe or the aperture is accomplished using stable, accurate translation stages, usually position-controlled with a laser interferometer. The quality of the edge (scattering centers), the degree of circularity, and the sensitivity to deformation are factors in the overall uncertainty, depending on which method is used. Advances in the metrology of aperture area measurement compared to the initial techniques available 25 years ago provided further motivation for this comparison.

2.2 NIST Method

The method adopted at NIST for measurement of aperture areas is a non-contact method, employing an interferometrically-controlled XY stage that translates the test sample, and a microscope with a CCD camera to locate the edge points. To perform the measurements, the aperture was mounted on a custom-made mounting ring. The system has been described previously.[16] It consists of a broadband light source illuminating the sample from below through a Kohler illuminator, an air-bearing-supported, an open-frame, XY stage with a heterodyne laser interferometer feedback system for XY-axes positioning, a Z-axis translation stage carrying a microscope with long working distance objectives, a digital CCD camera, and a control computer. Fig. 2 shows a photograph of the apparatus and Fig. 3 is an illustration of the instrument components. Characterization of the whole system and all its components was initially performed, including straightness of axis travel and squareness of the axis relative to each other. Only microscope alignment is performed routinely.

The automated data collection begins by finding the approximate geometric center of the aperture. The camera pixels are arbitrarily labeled, with the central pixel marked as the reference point for determining the *x, y* edge points. When an edge image is within the field of view, the XY stage is moved to bring the edge point to coincide with the central pixel. The number of pixels between the edge image's current pixel location and the center is converted to actual XY stage travel using the pixel length and magnification. The pixel arrays are scanned again after the move to determine the new edge location. This process is repeated until the edge is at or close to the central pixel. The fine positioning is completed when the distance becomes smaller than 25 nm, the minimum incremental movement of the stage. A final edge thresholding (the process of reading the gray levels of the central row of pixels) is performed to determine the coordinates of the edge point, as illustrated in Fig. 4. The total distance is the distance traveled by the stage plus the small amount determined from image metrology using the pixel sizes. The edge is assigned to be at 26.65 % of the gray level, as determined from coherence effects modeling of edge waveforms using commercial software.[17]

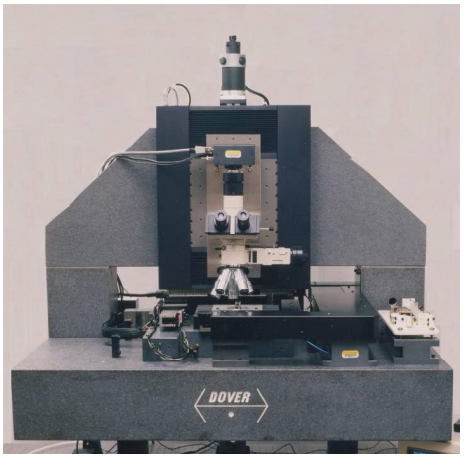

Figure 2. Photograph of the NIST absolute aperture measurement apparatus.

The Cartesian coordinates obtained from the automated data acquisition are used in a least-squares circle-fitting routine to determine the mean radius, and thus the geometric area. An ellipse-fitting routine is also used, mostly for comparative purposes. In the circle-fitting and ellipse-fittings routines, the bootstrap method is utilized to determine the standard "random plus form" uncertainty. The method involves repeated Monte Carlo resampling from a single data set to generate a standard deviation of the fitted radii.[18,19] For these samples, six measurements of 360 edge points each, at 1° angular interval, were performed for each aperture. The aperture was rotated between runs by 59.3°, to ensure the uniqueness of each data set. Replicate runs provide a measure of the reproducibility of the measurements and allow an assessment of the uncertainty due to defects in the edges.

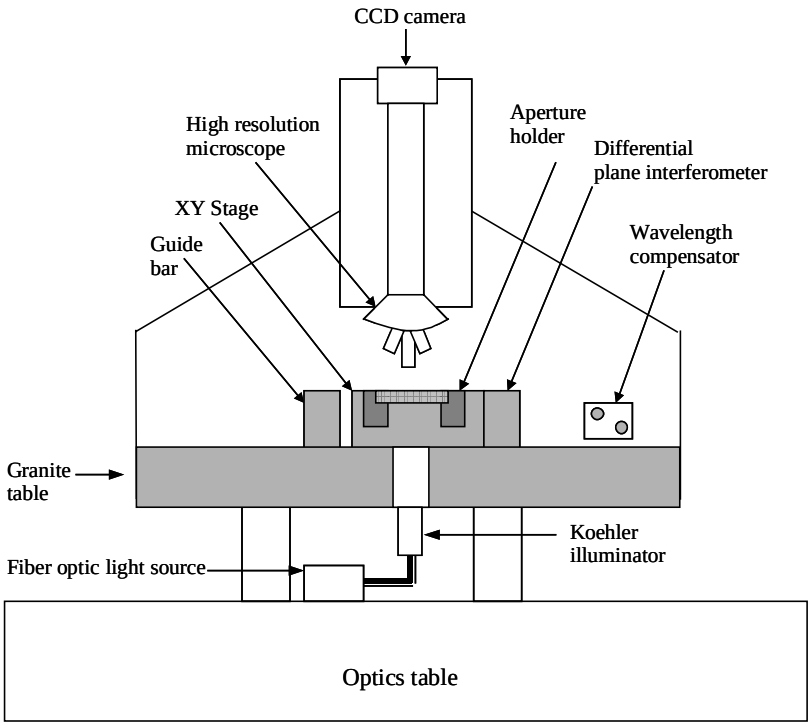

Figure 3. Layout of the absolute aperture measurement apparatus.

2.3 Uncertainty in Measurement Results

The present analysis yields the radius and area of the circle from the set of measurands, the coordinates of the edge points. The uncertainty in the radius and area requires an understanding of the uncertainty in the measured edge-point coordinates. (see Table 2)[20] The coordinates of an edge point, (x, y), are determined from the positional readings of the stage, *(XY)*, and from a subpixel length correction, *C*, associated with the edge-detection method,

$$x(y)_{\text{coordinate}} = X(Y)_{\text{stage}} \pm C\,. \tag{1}$$

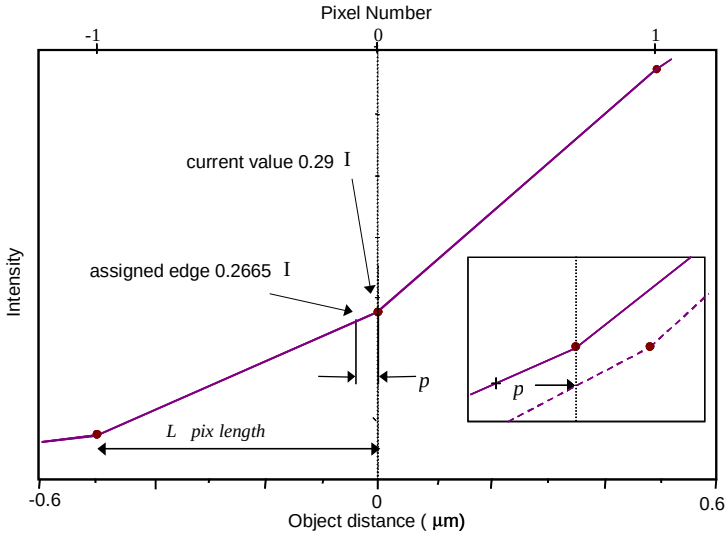

Figure 4. Illustration of the subpixel length correction. The assigned edge is predetermined to be at the 26.65 % of the illuminated area intensity. After final stage move, the edge may still not be at the center pixel. The length *p* is the fraction of pixel length the assigned edge is offset from the center.

The random plus form component (u_i) is the pooled standard deviation of the $6 \times N$ (typically, $N = 360$) total measurements of the aperture radius, and because of the large number of measurements is dominated by the form component, which specifies the non-circularity of the aperture. The Type A uncertainty ($k = 2$) on a single *x* or *y* measurement is approximately 50 nm, but contributes significantly less to the overall uncertainty due to the large number of coordinate measurements performed. The systematic uncertainties from the stage readings ($u_{j(\text{stage})}$) and from the image ($u_{j(\text{image})}$) are estimated.[20]

Uncertainty ($u_{j(t)}$) is due to the variation of the temperature over the course of the measurement. The highest temperature variation in the replicate runs was used to estimate the uncertainty in dimension due to thermal variation. The temperature variation during a measurement was at most, 0.3°C. There is uncertainty due to the geometry ($u_{j(g)}$) of the sample with respect to the instrument. This can be attributed to the non-planarity of the aperture edges upon mounting. The optimal focal positions of the microscope provide information on the location of the edges with respect to the XY (stage) plane. The maximum difference of focal positions between two diametrically opposite edge points is used to estimate the angular variation (θ) of the aperture with respect to the XY stage. A typical angular tilt is 0.3°. It should be noted that this does not take into account, warped sections, if any, of the aperture.

The combined uncertainty in the radius is the root-sum-of-squares of the various components.[21] There is a factor of four in the calculation because these components apply to the edge points, for *x* and *y* coordinates, while the total uncertainty is computed for radius.

$$u^2(R) = u_i^2 + 4u_{j(stage)}^2 + 4u_{j(image)}^2 + u_{j(t)}^2 + u_{j(g)}^2. \quad (2)$$

Table 2 presents a list of the sources of uncertainty and their contributions to the total relative uncertainty in the area for apertures with $R = 2.5$ mm and $R = 5.0$ mm. The systematic uncertainty of the XY stage is presently estimated based on the typical values for this type of stage and laser interferometer and awaits verification using a calibration grid plate appropriate for the size of the stage.

For measurements of total solar irradiance, the uncertainties for aperture area in Table 2 correspond to between 0.0089 % and 0.0082 % of the total solar irradiance (about 0.12 W/m^2). Such values are commensurate with scientific requirements. For example, the combined expanded uncertainty for the TIM on SORCE is 0.013 % and 0.016 %

(k = 2).[22] The largest components in the TIM uncertainty budget, aside from aperture area, are the uncertainties associated with diffraction and scattering, cavity reflectance, and optical-electrical equivalence.

Table 2. Sources of uncertainty and their nominal contributions for 5 mm and 10 mm diameter apertures

Uncertainty source		Quantity [nm]	u(R) [mm]	u(R)/R	u(A)/A	u(R) [mm]	u(R)/R	u(A)/A
Radius			2.5			5.0		
Random + form	u_i	25	2.50×10^{-5}	1.00×10^{-5}	2.00×10^{-5}	2.50×10^{-5}	5.00×10^{-6}	1.00×10^{-5}
Sys. Stage	$u_{j(\text{stage})}$	$2.6\times10^{-6}\times2R$	1.30×10^{-5}	5.20×10^{-6}	1.04×10^{-5}	2.60×10^{-5}	5.20×10^{-6}	1.04×10^{-5}
Sys. imaging	$u_{j(\text{image})}$	4	4.00×10^{-6}	1.60×10^{-6}	3.20×10^{-6}	4.00×10^{-6}	8.00×10^{-7}	1.60×10^{-6}
Thermal change	$u_{j(\text{t})}$	$0.3\times10^{-6}\times R$	7.50×10^{-6}	3.00×10^{-6}	6.00×10^{-6}	1.50×10^{-5}	3.00×10^{-6}	6.00×10^{-6}
Geometry	$u_{j(\text{g})}$	$\theta = 0.3$	3.43×10^{-5}	1.37×10^{-5}	2.74×10^{-5}	6.85×10^{-5}	1.37×10^{-5}	2.74×10^{-5}
TOTAL (k = 2)			1.02×10^{-4}	4.08×10^{-5}	8.15×10^{-5}	1.82×10^{-4}	3.65×10^{-5}	7.30×10^{-5}

3. PRELIMINARY RESULTS

To date, two laboratories have submitted apertures. We are awaiting submission from a third, and possibly a fourth laboratory. Because the results cannot be identified until the comparison is complete, we refer to the existing laboratories as Lab A and Lab B. Although they submitted unequal numbers of apertures, we have selected results so that equal numbers of apertures from each laboratory are presented. In this way, the results remain confidential, even to the participants to date. For similar reasons, we are unable to discuss in detail the design, heritage, previous measurements, and so forth for the apertures, although this will be examined in detail in the final paper. All of the measurements were corrected for thermal expansion to a reference temperature of 20 °C.

The preliminary results are shown in Fig. 5 for six apertures from each laboratory. The area, as reported by the laboratory, is normalized by the area determined by NIST and plotted as a function of aperture designation. The vertical lines correspond to the combined uncertainty in this ratio (k = 2), based on the uncertainties in area as reported by the participants and the uncertainties for the NIST measurements.

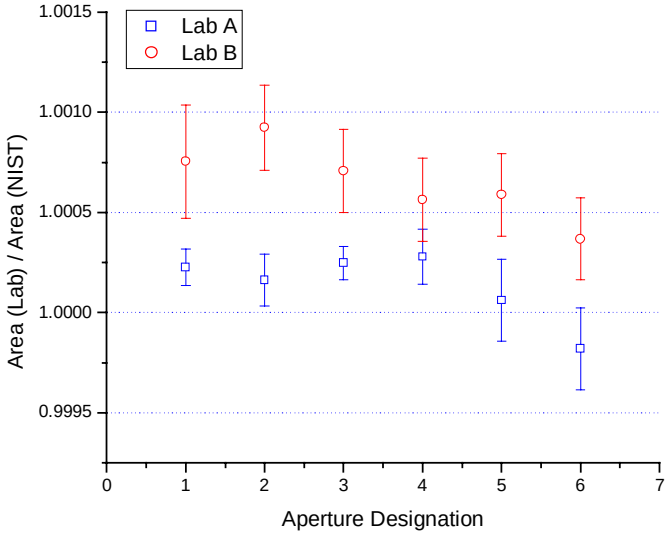

Figure 5. The preliminary results for two laboratories, shown as the ratio of the laboratory area to the area measured by NIST. The vertical lines correspond to the combined expanded uncertainties (k = 2).

The majority of the results in Fig. 5 are discrepant, if the uncertainties are properly estimated for the participant and NIST. Also, in nearly all of these cases, the laboratory overestimated the area according to the NIST results. For the selected results illustrated in Fig. 5, there appears to be a bias between the two laboratories when compared to NIST: the average ratio for Laboratory A is 0.013 % and the average ratio for Laboratory B is 0.065 %. This equates to a difference in total solar irradiance of 0.18 W/m^2 to 0.89 W/m^2 for a reference value of 1366.3 W/m^2.

4. CONCLUSIONS

The metrology of aperture area measurement has advanced since the beginning of observations of total solar irradiance from space 25 years ago, and new procedures exist for aperture manufacture and area measurement. In order to meet the scientific requirements, substantial effort must be expended on aperture area metrology. Small decreases in the output of the Sun (e.g., 0.1 %) are difficult to detect on an absolute scale but large enough to offset the effect on the Earth's climate from anthropogenic effects.[4] Discrepancies on the order of 0.04 % in successive solar minima, though small, are controversial and significant in the context of solar physics and global climate change.[3,23] The preliminary results reported here indicate that part of the offsets observed in total solar irradiance may be due to bias in the aperture area determinations. For future missions, cross-comparison of aperture area may be helpful in determining the change, if any, observed in the overall total solar irradiance.

5. ACKNOWLEDGMENTS

The authors are grateful to the participants who submitted apertures along with detailed background information. The work was supported by NASA's EOS Calibration/Validation program office.

6. REFERENCES

1. J. Lean, "The Sun's variable radiation and its relevance for Earth," *Ann. Rev. Astron. Astrophys.*, **35**, 33-67, 1997.
2. National Research Council, *Solar Influences on Global Change*, 163 pages, National Academy Press, Washington, DC, 1994.
3. C. Frohlich and J. Lean, "The Sun's total irradiance: Cycles, trends and related climate change uncertainties since 1976," *Geophys. Res. Lett.*, **25**, 4377-4380, 1998.
4. T. J. Quinn and C. Frohlich, "Accurate radiometers should measure the output of the Sun," *Nature*, **401**, 841-841, 1999.
5. J. J. Butler, "Calibration workshop for the Total Irradiance Monitor (TIM) instrument on the Earth Observing System's (EOS) Solar Radiation and Climate Experiment (SORCE)," *The Earth Observer*, **12**, 22-25, 2000.
6. J. J. Butler and B. C. Johnson, "Organization and implementation of calibration in the EOS project--part 1," *The Earth Observer*, **8**, 22-27, 1996.
7. J. J. Butler and B. C. Johnson, "Calibration in the EOS project part 2: implementation," *The Earth Observer*, **8**, 26-31, 1996.
8. E. A. Early, P. Y. Barnes, B. C. Johnson, J. J. Butler, C. J. Bruegge, S. F. Biggar, P. R. Spyak and M. M. Pavlov, "Bi-directional reflectance round-robin in support of the Earth Observing System Program," *J. Atmos. Oceanic Technol.*, **17**, 1077-1091, 2000.
9. J. E. Martin, N. P. Fox, N. J. Harrison, B. D. Shipp and M. Anklin, "Determination and comparisons of aperture areas using geometric and radiometric techniques," *Metrologia*, **35**, 461-464, 1998.
10. T. M. Goodman, J. E. Martin, B. D. Shipp and N. P. Turner, "The manufacture and measurement of precision apertures," *Inst. Phys. Conf. Ser.*, **92**, 121-128, 1988.
11. *Measurement of Qualified Plane Internal Diameters for Use as Master Rings and Ring Gauges*, The American Society of Mechanical Engineers, New York, NY, 1984.
12. J. B. Fowler and G. Deszi, "High accuracy measurement of aperture area relative to a standard known aperture," *J. Res. NIST*, **100**, 277-283, 1995.
13. J. Hartmann, "Advanced comparator method for measuring ultra-small aperture areas," *Meas. Sci. Tech.*, **12**, 1678-1682, 2001.
14. J. Fischer and M. Stock, "A non-contact measurement of radiometric apertures with an optical microtopography sensor," *Meas. Sci. Tech.*, **3**, 693-698, 1992.
15. A. Lassila, P. Toivanen and E. Ikonen, "An optical method for direct determination of the radiometric aperture area at high accuracy," *Meas. Sci. Tech.*, **8**, 973-977, 1997.

16. J. B. Fowler, R. S. Durvasula and A. C. Parr, "High-accuracy aperture-area measurement facilities at the National Institute of Standards and Technology," *Metrologia*, **35**, 497-500, 1998.
17. Metrologia, Spectel Research Corporation, Mountain View, CA. The software is only identified here to specify experimental procedure adequately. Such identification is not intended to imply recommendation or endorsement by the NIST nor is it intended to imply that the materials identified is necessarily the best available for the purpose.
18. B. Efron and R. Tibshirani, "Bootstrap methods for standard errors, confidence intervals, and other measures of statistical accuracy," *Statistical Science*, **1**, 54-77, 1986.
19. M. Litorja and I. Leonov. Natl. Inst. Stand. and Tech., Gaithersburg, MD, 2002.
20. J. B. Fowler and M. Litorja, "Geometric area measurement of circular apertures for radiometry at NIST," *Metrologia*, **40**, S9-S12, 2003.
21. B. N. Taylor and C. E. Kuyatt, *Guidelines for Evaluating and Expressing the Uncertainty of NIST Measurement Results*, NIST Tech. Note 1297, U. S. Department of Commerce, Gaithersburg, MD, 1994.
22. G. M. Lawrence, G. Kopp, G. Rottman, J. Harder, T. Woods and H. Loui, "Calibration of the Total Irradiance Monitor," *Metrologia*, **40**, S78-S80, 2003.
23. R. C. Willson, "Total solar irradiance trend during solar cycles 21 and 22," *Science*, **277**, 1963-1965, 1997.